Chemical Engineering Journal 106 (2005) 187–195

Chemical Engineering Journal

www.elsevier.com/locate/cej

Technical and economical evaluation of a zeolite membrane based heptane hydroisomerization process

M.L. Maloncy[a,*], Th. Maschmeyer[b], J.C. Jansen[a]

[a] *Ceramic Membrane Centre, The PORE, Delft University of Technology, Julianalaan 136, 2628 BL Delft, The Netherlands*
[b] *Centre for Molecular Catalysis, School of Chemistry, The University of Sydney, Sydney, NSW 2006, Australia*

Received 3 May 2004; accepted 25 November 2004

Abstract

An industrial scale heptane hydroisomerization process was simulated based on a concept of two reactors and a zeolite membrane. A product stream containing tribranched, and part of the dibranched C_7 isomers with octane number up to 92 is predicted. The economics of the process shows an investment cost of 40 million euros, with the membrane unit as the main cost driver. The technical and economical feasibility of this industrial scale heptane hydroisomerization process depends mainly on further development and performance of zeolite membranes.

Keywords: Hydroisomerization processes; Zeolite membranes; Heptane; Simulation

1. Introduction

Regulations to minimise the adverse impact of automotive fuel combustion on the environment have resulted in the need for changes in the automotive fuel composition worldwide. The challenge faced by refiners is to produce environmentally friendly gasoline with sufficiently high research octane number (RON). In the oil industry C_5 and C_6 paraffins are typically used in hydroisomerization units to obtain high octane number components. Paraffins larger than C_6, such as heptane are usually present in catalytic reforming feed streams and converted into aromatic compounds. Since regulation aims to reduce aromatic components in gasoline an alternative for the use of the higher alkanes is hydroisomerization. Besides the isomerization reaction the separation of high-octane value isomers from lower ones is also of great importance in the hydroisomerization process. There are numerous experimental efforts published on heptane isomerization, however, on heptane isomer separation literature data is scarce. Currently no commercially operating process for the hydroisomerization of heptane exists. In this work a preliminary design of a heptane hydroisomerization process using zeolite membrane is shown, aiming the production of high octane number heptane isomers. Besides the technical aspects of the process involving mainly the reaction and the membrane separation sections, the economics of the process is also evaluated. If essential data is missing in the early stage of process evaluation, reasonable assumptions have to be made, which of course have to be confirmed by experiments if the evaluation is favourable. Early feasibility studies, based on literature data, preliminary experiments or reasonable assumptions, are essential to identify the key parameters and to give guidance towards promising technologies [1].

2. Process concept

Nobel metal supported zeolite type catalysts are often used for *n*-heptane hydroisomerization. The selectivity towards heptane isomers using these catalysts depends on various factors such as: acid/metal site ratio [2] zeolite structure and zeolite acid strength [3,4]. If the catalyst is too acidic, cracking of mainly multibranched isomers is enhanced. On the other hand, if the catalyst is a too weak acid the isomerization may not proceed appropriately. For the hydroisomerization

* Corresponding author. Tel.: +31 152786197; fax: +31 152784289.
E-mail address: m.l.maloncy@tnw.tudelft.nl (M.L. Maloncy).

1385-8947/$ – see front matter © 2004 Elsevier B.V. All rights reserved.
doi:10.1016/j.cej.2004.11.011

Nomenclature

a_G	cross sectional area for gas flow (m^2)
a_L	cross sectional area for liquid flow (m^2)
a_M	membrane area (m^2)
$[A]$, $[B]$	concentration of component A and B ($mol\,m^{-3}$)
d	diameter of membrane tubes or monolith channel (m)
$E_{A,j}$, $E_{A,-j}$	activation energy of forward (j) and backward ($-j$) reaction ($kJ\,mol^{-1}$)
F_G	molar flow of gas stream ($mol\,s^{-1}$)
F_L	molar flow of liquid stream ($mol\,s^{-1}$)
J_i	flux of component i through membrane ($mol\,m^{-2}\,s^{-1}$)
$k_{0,j}$, $k_{0,-j}$	Arrhenius parameter of forward (j) and backward ($-j$) reaction (s^{-1})
k_C	rate constant of cracking (s^{-1})
k_{C0}	Arrhenius parameter for cracking reaction (s^{-1})
k_j	rate constant of reaction j (s^{-1})
K_j	equilibrium constant of reaction j, dimensionless
L	total length of membrane unit (m)
M	average molar mass of liquid stream ($mol\,kg^{-1}$)
n	number of membrane tubes or monolith channels
P	pressure in gas stream (Pa)
P_i^{sat}	pure component i vapour pressure in liquid stream (Pa)
r_C	rate of cracking ($mol\,m^{-3}\,s^{-1}$)
r_j	reaction rate of reaction j ($mol\,m^{-3}\,s^{-1}$)
R	ideal gas constant ($Pa\,m^3\,mol^{-1}\,K^{-1}$)
s	spacing of membrane tubes (m)
T	temperature (K)
u_G	velocity of gas stream ($m\,s^{-1}$)
u_L	velocity of liquid stream ($m\,s^{-1}$)
V	volume of membrane unit (m^3)
x_i	mole fraction of component i in liquid stream, dimensionless
y_i	mole fraction of component i in gas stream, dimensionless
z	axial space coordinate, dimensionless

Greek letters

β	constant, with value 2 for countercurrent and 1 for cross-flow configuration
γ_i	activity coefficient of component i in liquid stream, dimensionless
Π_i	permeance of component i ($mol\,m^{-2}\,s^{-1}\,Pa^{-1}$)
ρ	average density of liquid stream ($kg\,m^{-3}$)

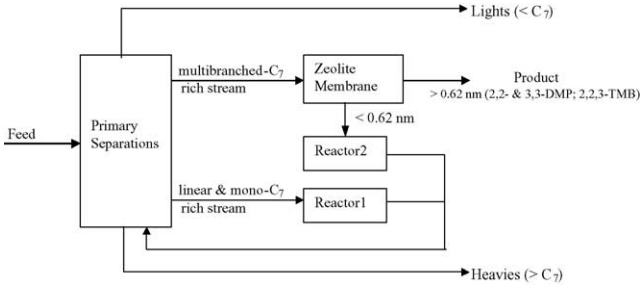

Fig. 1. Heptane hydroisomerization block scheme.

of *n*-heptane we propose a concept that uses two reactors, each with a different type of catalyst, and a separation unit composed of a zeolite membrane (see Fig. 1). The first reactor contains a strong acidic bifunctional type catalyst and aims to convert sequentially *n*-heptane to mono- and dibranched isomers. The second reactor is used to convert preferably 2,4-dimethylpentane into 2,2,3-trimethylbutane. According to the protonated cyclopropane (PCP) mechanism [5] 2,4-dimethylpentane is the main source for the formation of 2,2,3-trimethylbutane, the isomer with the highest RON (see Table 1). The catalyst used must be a moderate to weak acidic bifunctional type so that cracking of dibranched components is not enhanced while the formation of 2,2,3-TMB is promoted. Examples of catalysts for the first and second reactor are platinum loaded hydrogen-beta zeolite (Pt/H-BEA) type, which can have relatively high conversion and selectivity towards isomerization and less cracking [3], and nickel loaded on high area silica-alumina (Ni/ASA) type [9], respectively. The separation unit is used to separate the final product of the process composed of the dibranched 2,2-DMP, 3,3-DMP and tribranched 2,2,3-TMB, from smaller components, especially 2,4-DMP that is send to the second reactor. Separation by distillation is rather difficult as can be seen from the boiling point data in Table 1. A zeolite membrane with a channel aperture of approximately 0.52 nm × 0.58 nm in the orthorhombic phase [10] can be applied for this kind of separation. Assuming absolute separation within a perfect zeolite

Table 1
Kinetic diameter, boiling point and RON of heptane isomers

Component	Kinetic diameter (nm)[a]	Boiling point (K)	RON[b]
n-Heptane (*n*-C_7)	0.43	371.5	0.0
2-Methylhexane (2-MHx)	0.50	363.0	42.2
3-Methylhexane (3-MHx)	0.50	365.0	52.0
3-Ethylpentane (3-EP)	0.50	366.5	65.0
2,3-Dimethylpentane (2,3-DMP)	0.56	362.7	91.1
2,4-Dimethylpentane (2,4-DMP)	0.56	353.4	83.1
2,2-Dimethylpentane (2,2-DMP)	0.62	352.2	92.8
3,3-Dimethylpentane (3,3-DMP)	0.62	359.0	80.8
2,2,3-Trimethylbutane (2,2,3-TMB)	0.62	353.8	109.0

[a] [6,7].
[b] [8].

membrane, only the small molecules can permeate through the channel aperture. Thus, the di- and tribranched isomer products with their diameter of 0.62 nm will not enter the channels, while smaller molecules will permeate through the pores. Note that the values of the kinetic diameters given in Table 1 should be viewed as qualitative indications, since the concept of the kinetic diameter is based on simplified spherical representation and rigidity of a molecule or of a framework [11].

3. Process description and simulation

A process simulation was performed based on the proposed concept of two reactors and a separation unit. Fig. 1 shows the process block scheme. The process flow scheme has been previously presented [12,13] and is shown in Fig. 2. As feed to the process hydrogen was used as well as a simplified industrial naphtha feed with a RON of 57. The hydrocarbon feed contained C_6, C_7 and C_8 linear and branched alkanes. The C_7 components comprised about 40 wt.% of the feed. The throughput of the feedstock was assumed 907 metric tonne per day, comparable to that of existing C_5/C_6 isomerization processes (between 600 and 1200 metric tonne per day). The distillation train shown in Fig. 2 is composed of three distillation columns. The purpose of the first two columns is to separate the C_7 fraction from the heavier and lighter hydrocarbons, while the third column is used to separate the multibranched from the linear and monobranched C_7 components. The recycle stream is send via

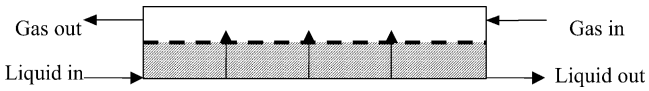

Fig. 3. Schematic view of the membrane unit.

a hydrogen separation membrane to the second distillation column. Within an overall refinery process, the lighter and heavier hydrocarbons separated in the distillation columns, could be used in state of the art C_5/C_6 hydroisomerization process and the reforming process, respectively.

Experimental data from [3] and [9] were used as a basis to obtain kinetic data. For hydroisomerization a first order reaction rate was assumed. The cracking reactions were assumed to be first order in reactant and zero order in hydrogen. The reaction models used are simple and do not increase simulation complexity.

For the membrane simulation a countercurrent pervaporation model was used. By using this model it is assumed that the individual components do not influence each other's fluxes. Fig. 3 shows a schematic view of the membrane unit. Permeance data were estimated from experiments performed in our laboratory [14] and also from the experimental work of Flanders et al. [15]. 2,3-DMP and 2,4-DMP were considered the slowest permeating components and the recovery of these species was set greater than 98% at the membrane outlet.

The reactor and membrane operation conditions set for process simulation are specified in Table 2. The process simulation was performed using Aspen and Excel, and different membrane design configurations were calculated.

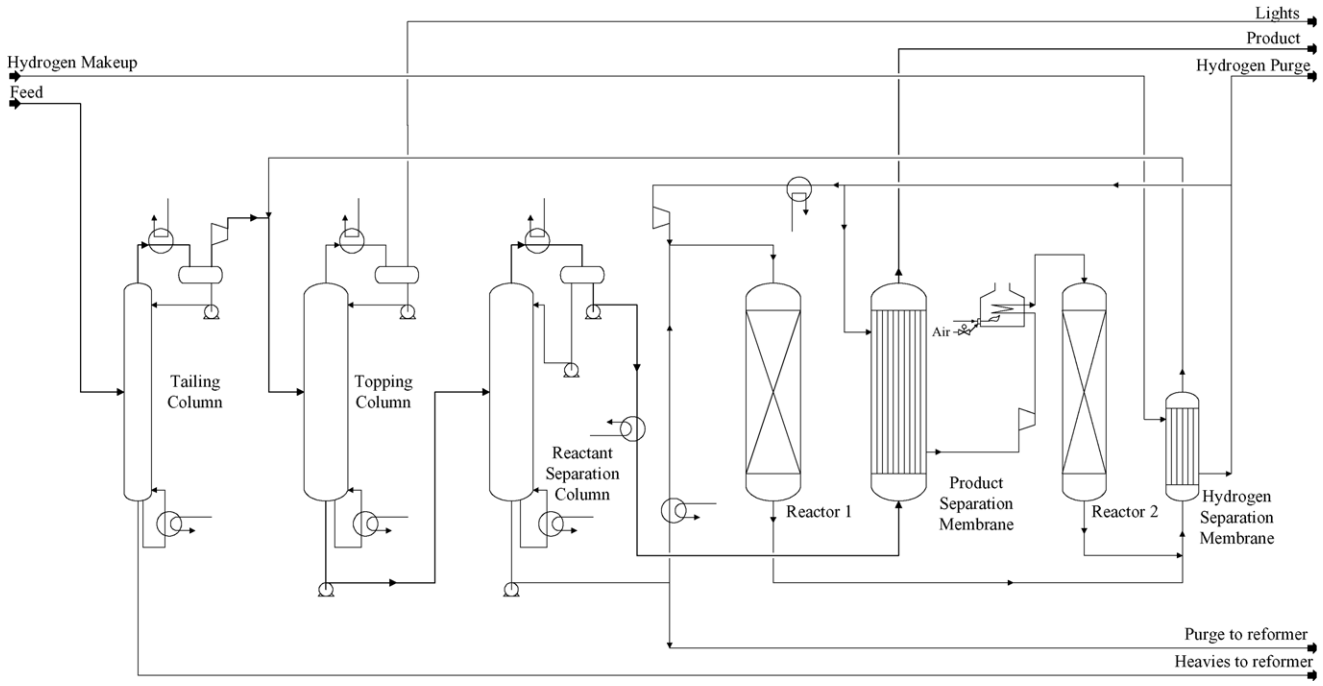

Fig. 2. Heptane process flow scheme.

Table 2
Reactor and membrane operation conditions

	Reactor 1	Reactor 2	Membrane
Reactor/membrane model	Plug flow adiabatic	Plug flow adiabatic	Countercurrent plug flow
Temperature (K)	473	573	458
Pressure ($\times 10^5$ Pa)	9.5	10	10 at feed side, 1 at permeate side
H_2/hydrocarbon molar ratio	8	4	–

4. Results and discussion

The focus of the results and discussion presented below will be mainly on the reactors, the product separation membrane and in lesser extend on the hydrogen separation membrane. The economics of the process will be highlighted as well.

4.1. Reactor design

Assuming the PCP mechanism for n-C_7 isomerization, the following reactions are mechanistically possible:

$$n\text{-}C_7 \leftrightarrow \text{2-MHx} \quad (1)$$

$$n\text{-}C_7 \leftrightarrow \text{3-MHx} \quad (2)$$

$$\text{2-MHx} \leftrightarrow \text{3-MHx} \quad (3)$$

$$\text{2-MHx} \leftrightarrow \text{2, 2-DMP} \quad (4)$$

$$\text{2-MHx} \leftrightarrow \text{2, 3-DMP} \quad (5)$$

$$\text{2-MHx} \leftrightarrow \text{2, 4-DMP} \quad (6)$$

$$\text{3-MHx} \leftrightarrow \text{2, 3-DMP} \quad (7)$$

$$\text{3-MHx} \leftrightarrow \text{3, 3-DMP} \quad (8)$$

$$\text{3-MHx} \leftrightarrow \text{3-EP} \quad (9)$$

$$\text{2, 2-DMP} \leftrightarrow \text{2, 3-DMP} \quad (10)$$

$$\text{2, 3-DMP} \leftrightarrow \text{2, 4-DMP} \quad (11)$$

$$\text{2, 3-DMP} \leftrightarrow \text{3, 3-DMP} \quad (12)$$

$$\text{2, 4-DMP} \leftrightarrow \text{2, 2, 3-TMB} \quad (13)$$

For the reactions (1)–(13) kinetic equations can be derived. For a reaction A ↔ B this equation holds:

$$r_j = k_j[A] - \frac{k_j}{K_j}[B] \quad (14)$$

K_j can be obtained from equilibrium compositions at the studied temperature. First order reaction rates were assumed. In literature first order reaction rate for hydroisomerization of heptane is described in the work of El Kady et al. [16]. Using a plug-flow reactor for process simulation, Arrhenius parameters and activation energy data were used as input:

$$k_j = k_{0,j} e^{-E_A/RT} \quad (15)$$

In Table 3 the Arrhenius parameters and activation energies of the forward and backward isomerization reactions used in the simulation are given.

Besides isomerization reactions cracking reactions were taken also into account, with mainly propane and isobutane as the cracking products. It is found in literature that multibranched isomers are preferably cracked and that hydroisomerization and cracking occurs in consecutive steps as shown in the reaction scheme below [17]:

$$n\text{-alkane} \rightleftarrows \text{MB} \rightleftarrows \text{MTB} \rightarrow \text{CR} \quad (16)$$

MB stands for single branched, MTB for multibranched and CR for cracked alkanes. The cracking reactions where assumed to be first order in reactant. The rate of cracking for a component A is given by:

$$r_C = k_C[A] \quad (17)$$

The cracking coefficient k_C is assumed to be only a function of the degree of branching:

$$k_{C,n\text{-}C_7} < k_{C,MB} < k_{C,MTB} \quad (18)$$

This assumption is valid for the first reactor that uses a stronger acidic catalyst with a relative high cracking ability. As input for the reactor simulation, the activation energy used for the cracking reactions was 175 kJ mol^{-1}. In Table 4 the Arrhenius parameters are given for the first reactor. Because of the moderate acid catalyst used the cracking ability of the second reactor should be lower, using therefore the Arrhenius parameter of 1.56×10^{12} s^{-1} for all reactant, excluding n-C_7 ($k_{C0} = 0$ s^{-1}). Zero order in hydrogen was assumed in the reactions. Simulations using the reaction models within a plug flow reactor consideration resulted in the product distribution of the reactors effluent given in Table 5. The total amount of feed to the first and second reactor was 1813 and 1033 metric tonne per day, respectively. The estimated amount of catalyst and the reactors dimensions together with other reactor specifications are given in Table 6. Because of their large scale and ease of design and operability, both reactors used in the process, are fixed bed reactors. The short residence time distribution of these reactors favours a high selectivity. Both reactors are operated adiabatic and in gas phase.

4.2. Membrane design

A countercurrent membrane pervaporation model is used for the membrane design. In pervaporation, the driving force is the difference in partial pressure on the gas side and the

Table 3
Arrenhius parameters k_0 and activating energies E_A for forward (j) and backward ($-j$) isomerization reactions

Reaction	k_0 ($\times 10^{12}$ s^{-1}) (reactor 1)		k_0 ($\times 10^{8}$ s^{-1}) (reactor 2)		E_A (kJ mol^{-1})	
	$k_{0,j}$	$k_{0,-j}$	$k_{0,j}$	$k_{0,-j}$	$E_{A,j}$	$E_{A,-j}$
(1)	43.30	96.40	26.60	65.30	135.5	142.2
(2)	52.90	64.60	0.09	0.11	136.3	139.8
(3)	71.40	39.20	48.40	24.00	139.3	136.0
(4)	3.560	71.40	0.01	0.29	131.2	141.5
(5)	32.10	71.40	0.06	0.13	137.7	137.4
(6)	10.70	107.00	6.55	72.20	133.5	139.1
(7)	9.67	39.20	0.04	0.16	135.6	138.5
(8)	0.53	10.70	26.60	590.00	131.7	139.4
(9)	0.08	13.10	4.39	652.00	126.6	139.4
(10)	87.30	0.87	0.36	0.03	143.7	133.2
(11)	23.80	107.00	108.00	483.0	134.5	140.3
(12)	19.50	96.40	88.20	483.00	134.6	139.3
(13)	71.40	21.50	796.00	217.00	146.1	135.4

Table 4
Arrenhius parameters used for cracking reaction (k_{C0}) in the first reactor

Reactant	k_{C0} ($\times 10^{16}$ s^{-1})
Linear n-C_7	5.59
Monobranched	7.56
Dibranched	17.90
Tribranched	40.50

vapour pressure on the liquid side of the membrane. The flux in pervaporation can be calculated using the driving force and the permeance value of the specific component for the specific membrane. By using this model it is assumed that the individual components do not influence each other's fluxes.

$$J_i = \Pi_i(x_i\gamma_i P_i^{\text{sat}} - y_i P) \tag{19}$$

The mass balances can be specified using the countercurrent plug-flow model (Fig. 3). Both the composition and the total flow of both streams change and have to be integrated over the length of the membrane.

Table 5
Reactor product distribution (wt.%)

	Reactor 1		Reactor 2	
	Feed	Product	Feed	Product
H_2	13.8	13.7	7.5	7.4
Propane	0.0	3.5	0.0	0.5
Isobutane	0.0	4.6	0.0	0.7
n-C_7	22.2	11.4	3.4	4.6
2-MHx	24.1	20.9	30.3	29.0
3-MHx	25.0	20.2	19.2	18.2
2,2-DMP	0.0	5.7	0.0	0.0
2,3-DMP	9.3	6.6	12.0	14.1
2,4-DMP	0.1	6.0	24.9	14.6
3,3-DMP	1.6	3.4	0.0	4.2
3-EP	2.7	2.5	1.4	1.6
2,2,3-TMB	0.0	0.4	0.0	3.7
Others	1.2	1.1	1.3	1.4

Table 6
Reactor specifications

	Reactor 1	Reactor 2
Reactor type	Fixed bed adiabatic	Fixed bed adiabatic
Temperature (K)	473	573
Pressure ($\times 10^5$ Pa)	9.5	10
Pressure drop ($\times 10^5$ Pa m^{-1})	0.06	0.025
Length (m)	14	14
Diameter (m)	3.7	4.2
Catalyst	Pt/H-BEA (0.5 wt.% Pt)	Ni/ASA (5 wt.% Ni)
Catalyst mass (metric tonne)	150	194
D_p (m)	0.003 (sphere)	0.001 (sphere)

Component balance for the liquid stream:

$$\frac{\mathrm{d}(F_L x_i)}{\mathrm{d}z} = \Pi_i(x_i\gamma_i P_i^{\text{sat}} - y_i P)a_M \tag{20}$$

Component balance for the gas stream:

$$\frac{\mathrm{d}(F_G y_i)}{\mathrm{d}z} = \Pi_i(x_i\gamma_i P_i^{\text{sat}} - y_i P)a_M \tag{21}$$

And the total mass balance:

$$\frac{\mathrm{d}F_L}{\mathrm{d}z} = \frac{\mathrm{d}F_G}{\mathrm{d}z} = \sum_i \Pi_i(x_i\gamma_i P_i^{\text{sat}} - y_i P)a_M \tag{22}$$

Evaluation of the mass balance equations yields the required membrane area (a_M). To evaluate these equations permeance data for the components is required. Vapour permeation experiments performed in our laboratory with C_7 mixtures gave at 353 K permeance values of 4.0×10^{-10} mol m^{-2} s^{-1} Pa^{-1} for 2,4-DMP and 4.4×10^{-8} mol m^{-2} s^{-1} Pa^{-1} for linear C_7. At a temperature of 393 K the double branched permeance was 1.6×10^{-9} mol m^{-2} s^{-1} Pa^{-1} and the linear C_7 permeance was 7.7×10^{-8} mol m^{-2} s^{-1} Pa^{-1} [14]. An increase of permeance with increasing temperature was observed for the double branched and the linear heptane. A silicalite-1 membrane with a thickness of about 16×10^3 nm was used.

Literature data on the separation of heptane isomers is scarce making it difficult to compare our data with literature. However, when comparing with literature data of C_6, the permeances are in the same order of magnitude [15]. Flanders et al. [15] compared pervaporation with vapour permeation and their results showed that the double-branched permeance for pervaporation was an order of magnitude higher than vapour permeation. The authors also observed relative constant permeance behaviour of the dibranched components with increased driving force. If we extend those finding to our work, the permeance of the 2,4-DMP would be in the order of 10^{-8} applying pervaporation. So, in the equations permeance of 1×10^{-8} mol m^{-2} s^{-1} Pa^{-1} for the double-branched components was used. For the boundary conditions at the inlet, the process streams coming from the distillation column and the hydrogen separation membrane were used (see Fig. 2). Mainly multibranched components were considered with 2,3-DMP and 2,4-DMP as the slowest permeating species. The boundary condition set at the outlet was that the recovery of the slowest permeating species should not be greater than 98%. The vapour pressure of 8.0×10^5 and 9.8×10^5 Pa for 2,3-DMP and 2,4-DMP were used, respectively, at the operation temperature of 458 K. The solution of the equations yields a membrane area of about 20,000 m^2. Meindersma and de Haan [18] in their work on aromatic compounds separation using zeolite membranes estimated membrane areas ranging from 60,800 to 136,500 m^2 depending on the purity requirement. A feed of 300 metric tonne per hour was used in their work, which is about six times higher than the amount of feed sent to the membrane unit of the present work. The estimated membrane areas given above are currently not produced commercially for zeolite membrane units. The first large-scale pervaporation plant using zeolite membrane put into industrial operation has a total membrane area of about 60 m^2 [19]. The zeolite that is used is the NaA-type zeolite. The feed flow to the pervaporation plant is 0.48 metric tonne per hour with water content of 10 wt.%. Thus, the technical feasibility of the proposed *n*-heptane process in this work is restricted by further development of zeolite membranes on a larger scale.

For the calculation of the dimensions of the membrane unit different geometries can be used to apply membrane technology in industrial practice. The most straightforward solution is the shell and tube configuration (Fig. 4a). It is similar to a countercurrent heat exchanger but here mass is exchanged. One of the disadvantages is the large internal volume of the unit (low membrane surface to unit volume ratio). Monolith structures, however, have a very high surface to volume ratio. They consist of a large number of parallel square channels with sizes ranging from 10 to 100 cells per square inch. Research of MFI type membranes on monolith used to separate light alkanes is already in development [20–22]. Although in theory these structures can be applied in countercurrent mode (Fig. 4b) it will have practical difficulties to connect all individual channels to the corresponding process streams. A feasible solution is the use of cross-flow monolith structures

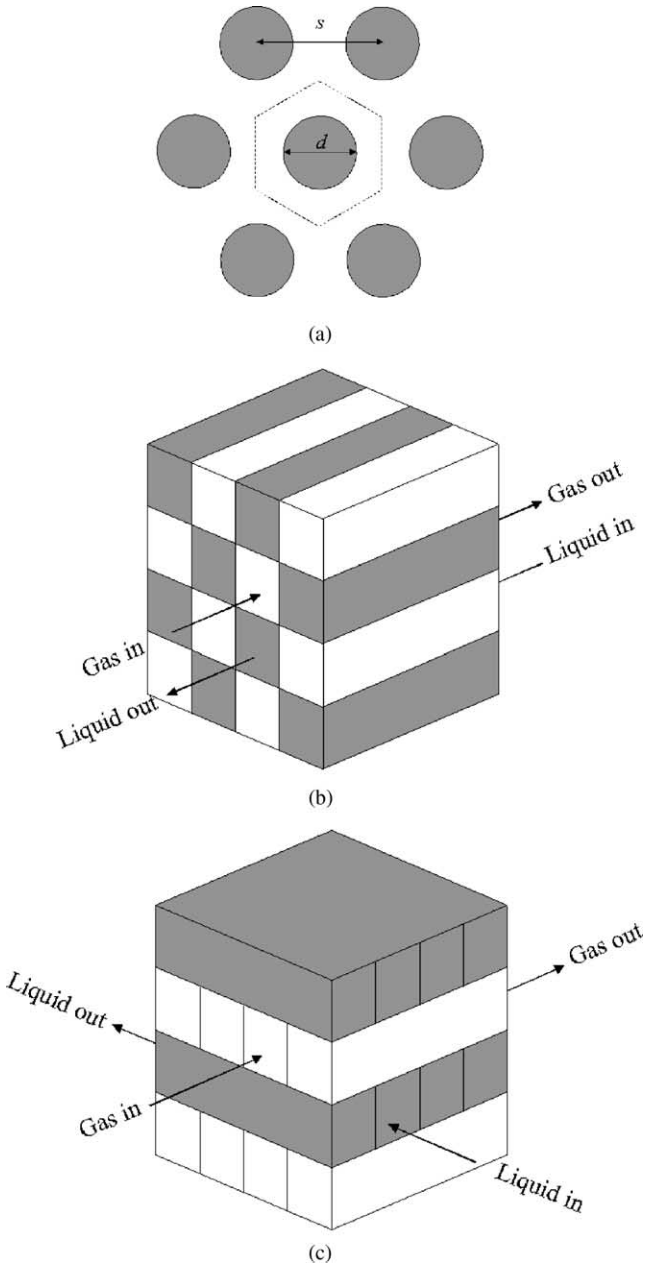

Fig. 4. Different membrane configurations: (a) shell and tube membrane unit (top view); (b) countercurrent monolith; (c) cross-flow monolith. The dark areas indicate liquid flow inside the tube/channels.

[23,24] shown in Fig. 4c. In this structure cross flow can be established because each layer of channels is rotated by 90°. By interconnecting multiple units one can approach countercurrent operation. The dimensions of the shell and tube configuration are calculated as follows (liquid flow inside the tubes):

$$n = \frac{a_M}{\pi \, dL} \tag{23}$$

$$a_L = \frac{\pi}{4} d^2 n \tag{24}$$

$$a_G = \frac{\sqrt{3}}{2}s^2 n - \frac{\pi}{4}d^2 n \quad (25)$$

$$V = (a_L + a_G)L \quad (26)$$

For both monolith configurations the equations are:

$$n = \frac{a_M}{\beta\, dL} \quad (27)$$

$$a_L = a_G = \tfrac{1}{2}d^2 n \quad (28)$$

$$V = (a_L + a_G)L \quad (29)$$

Of course, the smaller the tube or channel diameter (d), the higher the surface to volume ratio will be. This results in a very compact membrane unit design. However, by narrowing the tubes, gas and liquid velocities will increase and so will the pressure drop. This is an important factor for designing membrane units. The liquid velocity is calculated as follows:

$$u_L = \frac{F_L M}{\rho a_L} \quad (30)$$

And for the gas velocity:

$$u_G = \frac{F_G RT}{P a_G} \quad (31)$$

In the present work the limiting factors are not the fluid velocities but the minimal dimensions of current membrane units. For industrial tubes this is around 1 in. tube diameter and for monoliths about 0.0025 m channel size. The results of the calculations are shown in Table 7. For the shell and tube option a total volume of 62 m^3 is estimated. Four units with a length of 10 m are required, each unit containing 6400 tubes of 1 in. diameter. For the cross-flow monolith option a total volume of 50 m^3 of monolith units with 0.0025 m channels is required. In this case the liquid velocity is 0.0015 m s^{-1} and the gas velocity is 2.2 m s^{-1}. The Reynolds number on the gas side is about 1650, indicating a low pressure drop. As the cross-flow structure gives more favourable results than the shell and tube structure, it was chosen in the design.

For the hydrogen separation membrane a gas separation model was used. Permeance data for hydrogen was obtained from [25]. The authors used silica membranes with a thickness of 30 nm. The hydrogen permeance was about 2×10^{-6} mol m^{-2} s^{-1} Pa^{-1} at temperatures around 473 K. Methane permeance was more than 500 times smaller, and molecules larger than methane were completely blocked. On the assumption that the same type of membrane is used in the present work, thus only hydrogen permeates through the membrane, and applying the permeance data of [25], a membrane area of around 4000 m^2 was estimated. The pressures at the feed and the permeate side of the membrane were 8.6×10^5 and 5.6×10^5 Pa, respectively. The operation temperature of the membrane was 506 K. For the design of the hydrogen separation membrane a cross-flow monolith membrane was considered. The estimated dimensions are given in Table 8.

Table 7
Specifications for two types of membrane configurations

	Shell and tube system	Cross-flow monolith
Membrane area	20,000 m^2	20,000 m^2
Channel size	0.025 m (tube i.d.)	0.0025 m (100 CPSI)
No. of units	4	1
No. of channels per unit	6366 tubes	2×10^6 channels
Unit volume	62 m^3	50 m^3
Unit dimensions ($L \times D$ or $L \times W \times H$)	10 m × 2.8 m	4 m × 4 m × 3.1 m
Liquid velocity	0.0007 m s^{-1}	0.0015 m s^{-1}
Gas velocity	1.0 m s^{-1}	2.2 m s^{-1}
Reynolds number (gas)	7500	1650

Table 8
Specification of the hydrogen separation membrane

Membrane type	Cross-flow monolith
Membrane area	3647 m^2
Channel size	0.002 m
No. of channels	6.1×10^5 channels
Unit volume	7.3 m^3
Gas velocity	4.4 m s^{-1}
Reynolds number (gas)	1878

4.3. Overall simulation

The total process simulation with the 907 metric tonne per day of feedstock resulted in 220 metric tonne per day of product with RON of 92 containing mainly 2,2,3-TMB, 2,2-DMP and 3,3-DMP with a weight composition of 19, 46 and 34%, respectively. The amount of product compared to the feed is rather low, about 24%, because of the initial separation of C_6 and C_8 components. However, there was a RON upgrading of 35 points from feed to product.

4.4. Economics

Simple measurements of cost estimation were used to evaluate the process economics. The total investment was calculated as the sum of the fixed and working capital. Using the Lang factorial method the fixed capital (C_f) is estimated as a function of the total purchase cost of equipments (PCE) [26].

$$C_f = 3.7\,\mathrm{PCE} \quad (32)$$

The PCE cost estimated is 9.5 million euros. The cost distribution is shown in Fig. 5. The fixed capital cost estimated is 35 million euros. Considering the working capital 15% of the fixed capital, the total investment will be 40 million euros. This value is much higher compared to those reported in [27] for different C_5/C_6 hydroisomerization plants. As an example, a UOP Penex/Molex plant with a similar feed processing capacity has an investment of about 23 million euros. The main cost driver as can be seen from Fig. 5 is the membrane. The price per square meter of membrane was set 200 euros, which is around 10% of the value of currently commercialised zeolite A type membranes [28], on the assumption

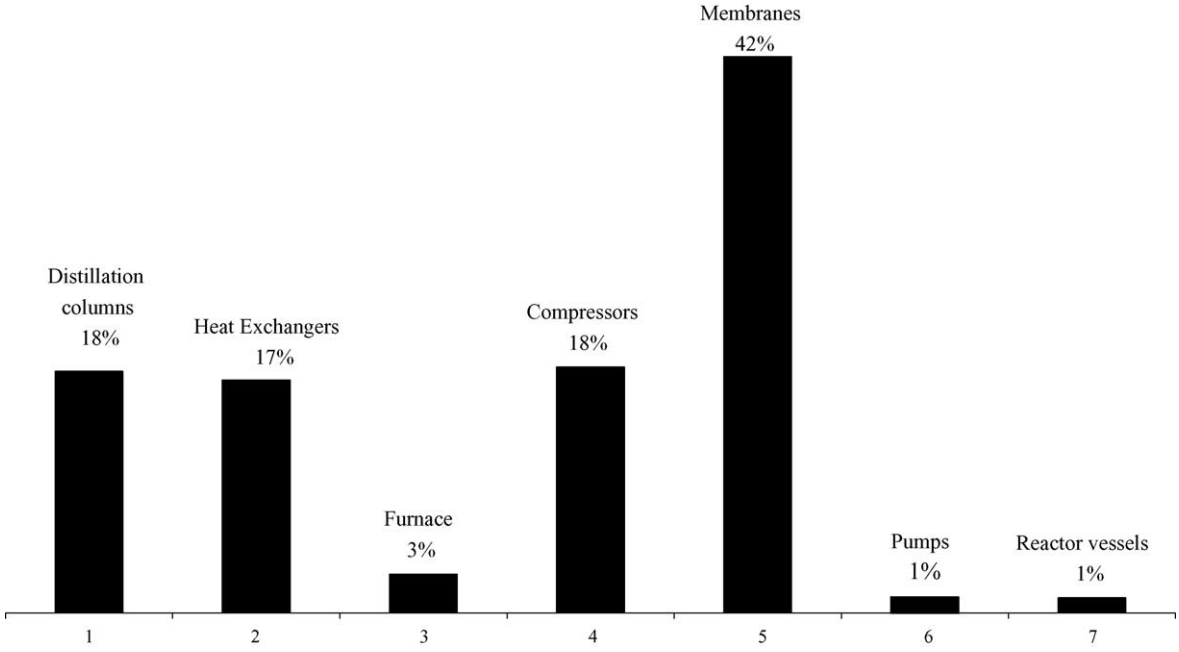

Fig. 5. Equipment cost distribution.

that future progress made on zeolite membrane module installation will reduced the cost by a factor of around 10. A more economically feasible situation would be if the development on zeolite membrane modules would reach the same stage as for polymer membrane reducing the price to values around 20–25 euros per square meter, which is currently the price for state of the art, hollow fibre modules [29].

To visualise the financial impact of the different items on the process a product based cost (cash) factor scheme is set up and shown in Fig. 6. The factors are defined as the total price (cost) of determined item divided by the total price of the product. The items going into the process are the cost, while those coming out provide the cash. The process feed has a high impact on the cost. This is basically because of the low product yield of the process. 4.1 metric tonne of feed is used to produce 1 metric tonne of product. In contrast the importance of the by-products in providing cash is shown by its factor of 1.85. The impact of the utilities is significant as well. Further optimisation can reduce a lot in i.e. steam and electricity usage. Moreover, the investment and operation

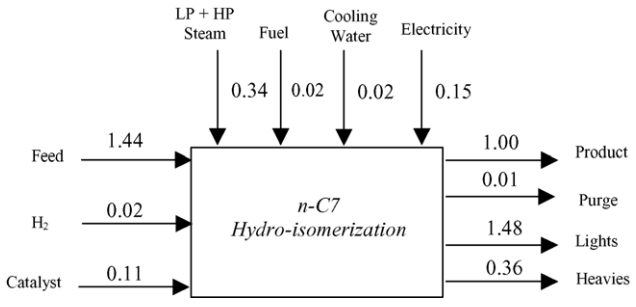

Fig. 6. Product based cost (cash) factor scheme.

costs may be affected significantly, increasing the economic viability of the process.

5. Concluding remarks

Using a simplified feed, reaction and separation data a design of a heptane hydroisomerization process is developed. A total amount of 907 metric tonne per day of feed is processed from which 220 metric tonne per day of product is formed. This is a low product yield, however, there is an improvement in research octane number from 57 up to 92. The investment cost of the process is 40 million euros, which is higher than state of the art C_5/C_6 hydroisomerization processes. The limitations of the design are the relatively simple models used to simulate the reactors and membranes. For the first heptane hydroisomerization process to be operational a few bottlenecks in the process development have to be solved. These include: (1) controlling hydroisomerization versus hydrocracking, (2) separation of mono- from multibranched isomers and (3) development on industrial scale of large surface area, high quality (MFI) zeolite membranes. Furthermore, the importance of hydrogen for the process should be further explored. Hydrogen affects the hydroisomerization/cracking reactions. A low amount of hydrogen sufficient enough to promote isomerization and suppress cracking could reduce reactor volume and mainly compressor duty, decreasing utility cost. In the design no consideration was made with respect to cyclic compounds, however investigation on the influence of cyclic compounds is important since these compounds are generally present in naphtha feed streams. As there is space for optimisation, a heptane hydroisomerization process containing the concept of two reactor and a membrane has potential for RON

upgrading and could be extended to process a larger range of hydrocarbon such as C_5/C_6 and heavier naphtha. This would provide higher product yields than predicted in the present work.

Acknowledgements

V.F.M. Tjon Soei Len, B.M. Vogelaar, M.A. Rijkse, E.S.E.D. van Kints and L. Gora are gratefully acknowledged for their contribution.

References

[1] G.W. Meindersma, Preliminary cost evaluation: the most forgotten aspect in developing processes, NPT Procestechnologie 9 (5) (2002) 19–23.
[2] T.F. Degnan, C.R. Kennedy, Impact of catalyst acid/metal balance in hydroisomerization of normal paraffins, AIChE J. 39 (4) (1993) 607–614.
[3] K.-J. Chao, H.-C. Wu, L.-J. Leu, Hydroisomerization of light normal paraffins over series of platinum-loaded mordenite and beta catalysts, Appl. Catal. A 143 (1996) 223–243.
[4] A. Patrigeon, E. Benazzi, Ch. Travers, J.Y. Bernard, Influence of the zeolite structure and acidity on the hydroisomerization of *n*-heptane, Catal. Today 65 (2001) 149–155.
[5] S.T. Sie, Acid-catalyzed cracking of paraffinic hydrocarbons. 3. Evidence for the protonated cyclopropane mechanism from hydrocracking/hydroisomerization experiments, Ind. Eng. Chem. Res. 32 (1993) 403–408.
[6] D.W. Breck, Zeolite Molecular Sieves: Structure, Chemistry, and Use, Wiley, New York, 1974.
[7] H.H. Funke, A.M. Argo, J.L. Falconer, R.D. Noble, Separation of cyclic, branched and linear hydrocarbon mixtures through silicalite-1 membranes, Ind. Eng. Chem. Res. 36 (1997) 137–143.
[8] W.G. Lovell, Knocking characteristics of hydrocarbons, Ind. Eng. Chem. Res. 40 (1948) 2388.
[9] F.G. Ciapetta, J.B. Hunter, Isomerization of saturated hydrocarbons in presence of hydrogenation-cracking catalysts, Ind. Eng. Chem. 45 (1) (1953) 147–165.
[10] H. van Koningsveld, J.C. Jansen, H. van Bekkum, The monoclinic framework structure of zeolite H-ZSM-5. Comparison with the orthorhombic framework of as-synthesized ZSM-5, Zeolites 10 (1990) 235–242.
[11] H. Jobic, Diffusion of linear and branched alkanes in ZSM-5. A quasi-elastic neutron scattering study, J. Mol. Catal. A: Chem. 158 (2000) 135–142.
[12] M.L. Maloncy, J.C. Jansen, Th. Maschmeyer, *n*-Heptane hydroisomerization using zeolite membrane separation technology, in: Annual Symposium on Zeolitic Materials, Belgium, 2001, pp. 40–41.
[13] M.L. Maloncy, J.C. Jansen, Th. Maschmeyer, A conceptual design of a *n*-heptane hydroisomerization process, in: Proceedings of the XVIII Iberoamerican Symposium on Catalysis, Venezuela, 2002, pp. 553–558.
[14] M.L. Maloncy, L. Gora, J.C. Jansen, Th. Maschmeyer, The separation of branched heptane from normal heptane using a zeolite membrane, in: Proceedings of the Fourth European Congress of Chemical Engineering, Spain, 2003, CD-ROM.
[15] C.L. Flanders, V.A. Tuan, R.D. Noble, J.L. Falconer, Separation of C_6 isomers by vapor permeation and pervaporation through ZSM-5 membranes, J. Membr. Sci. 176 (2000) 43–53.
[16] F.Y.A. El Kady, M.F. Menoufy, H.A. Hassan, Reaction mechanism and order rate of *n*-heptane isomerization, Indian J. Technol. 21 (1983) 300–305.
[17] J.F. Denayer, G.V. Baron, W. Souverijns, J.A. Martens, P.A. Jacobs, Hydrocracking of *n*-alkane mixtures on Pt/H-Y zeolite: chain length dependence of the adsorption and the kinetic constants, Ind. Eng. Chem. Res. 36 (1997) 3242–3247.
[18] G.W. Meindersma, A.B. de Haan, Economical feasibility of zeolite membranes for industrial scale separations of aromatic hydrocarbons, Desalination 149 (2002) 29–34.
[19] Y. Morigami, M. Kondo, J. Abe, H. Kita, K. Okamoto, The first large-scale pervaporation plant using tubular-type module with zeolite NaA membrane, Sep. Purif. Technol. 25 (2001) 251–260.
[20] H. Kalipcilar, J.L. Falconer, R.D. Noble, Preparation of B-ZSM-5 membranes on monolith support, J. Membr. Sci. 194 (2001) 141–144.
[21] H. Kalipcilar, S.K. Gade, R.D. Noble, J.L. Falconer, Synthesis and separation of B-ZSM-5 membranes on monolith supports, J. Membr. Sci. 210 (2002) 113–127.
[22] T.C. Bowen, H. Kalipcilar, J.L. Falconer, R.D. Noble, Separation of C_4 and C_6 isomer mixtures and alcohol–water solutions by monolith supported B-ZSM-5 membranes, Desalination 147 (2002) 331–332.
[23] C.G. Vayenas, P.G. Debenedetti, I. Yentekakis, L.L. Hegedus, Cross-flow, solid state electrochemical reactors: a steady-state analysis, Ind. Eng. Chem. Fundam. 24 (1985) 316–324.
[24] S.G. Neophytides, The reversed flow operation of a crossflow solid oxide fuel cell monolith, Chem. Eng. Sci. 54 (1999) 4603–4613.
[25] R.M. de Vos, H. Verweij, High-selectivity, high-flux silica membranes for gas separation, Science 279 (1998) 1710–1711.
[26] R.K. Sinnott, Coulson and Richardson Chemical Engineering, Chemical Engineering Design, vol. 6, Butterworth-Heinemann, Oxford, 1993, pp. 212–245.
[27] Special Report Refining Processes ’98, Hydrocarbon Processing: International edition, vol. 77, 11 November 1998, pp. 98–104.
[28] J. Caro, M. Noack, P. Kölsch, R. Schäfer, Zeolite membranes—state of their development and perspective, Microporous Mesoporous Mater. 38 (2000) 3–24.
[29] S.R. Tennison, Economical perspectives/analysis of the application of zeolite and microporous membranes, in: Proceedings of the International Workshop on Zeolitic and Microporous Membranes, Purmerend, The Netherlands, 2001, pp. 55–58.